

Characterization of Parity-Time Symmetry in Photonic Lattices Using Heesh-Shubnikov Group Theory

Adam Mock*

*School of Engineering and Technology, Central Michigan University, ET 100, Mount Pleasant, MI 48859, USA
and Science of Advanced Materials Program Central Michigan University, Mount Pleasant, MI 48859, USA*

(Dated: June 17, 2016)

We investigate the properties of parity-time symmetric periodic photonic structures using Heesh-Shubnikov group theory. Classical group theory cannot be used to categorize the symmetry of the eigenmodes because the time-inversion operator is antiunitary. Fortunately, corepresentations of Heesh-Shubnikov groups have been developed to characterize the effect of antiunitary operators on eigenfunctions. Using the example structure of a one-dimensional photonic lattice, we identify the corepresentations of eigenmodes at both low and high symmetry points in the photonic band diagram. We find that thresholdless parity-time transitions are associated with particular classes of corepresentations. The approach is completely general and can be applied to parity-time symmetric photonic lattices of any dimension. The predictive power of this approach provides a powerful design tool for parity-time symmetric photonic device design.

Recently it has been shown that non-Hermitian Hamiltonians that are invariant under the combined operation of parity (\mathcal{P}) and time-inversion (\mathcal{T}) possess either real eigenvalues or sets of paired complex conjugate eigenvalues [1–3]. Whether an eigenstate of such a Hamiltonian has a real or complex eigenvalue depends on (i) the precise spatial symmetry of the non-Hermitian potential and (ii) the degree of non-Hermiticity. In this study we focus on (i) and apply Heesh-Shubnikov [4, 5] group theory to electromagnetic systems with \mathcal{PT} symmetry to determine which states are expected to have real or complex eigenvalues. Because the conclusions are based entirely on symmetry and not on the degree of non-Hermiticity as in (ii), we expect the eigenvalues to maintain their realness or complexity even in the limit of infinitesimal non-Hermiticity. Previously, the existence of complex conjugate eigenvalues with infinitesimal non-Hermiticity has been referred to as thresholdless \mathcal{PT} symmetry breaking. However, because such a situation arises as a direct result of the particular symmetry of the Hamiltonian, a more accurate descriptor would be two-fold \mathcal{PT} -degeneracy (n -fold if more than two eigenmodes with complex conjugate eigenvalues are involved). Note that these modes are not rigorously degenerate because only the real part of their eigenfrequencies are equal. When the eigenvalue of an eigenstate changes from real to complex as a function of the non-Hermiticity factor (as in (ii)), then the \mathcal{PT} symmetry has been broken.

Electromagnetics has proven a fruitful platform for exploring the consequences of \mathcal{PT} symmetric Hamiltonians [6–20]. A \mathcal{PT} symmetric electromagnetic Hamiltonian can be created with appropriate spatial arrangements of regions in which electromagnetic waves experience gain or loss. The gain and loss appear in the time-harmonic Maxwell equations as a complex index of refraction $n = n_r \pm in_i$ (+ for gain, – for loss), and the imaginary part n_i is the non-Hermiticity factor. Recent studies have shown that the modes of spatially periodic

structures with \mathcal{PT} symmetry exhibit a wide variety of behavior that depends on their location on a band diagram: modes can be non-degenerate, “classically degenerate” or \mathcal{PT} -degenerate, and the \mathcal{PT} -degeneracy can be thresholdless or be a function of a non-Hermiticity factor [21–41]. Presently we investigate the \mathcal{PT} symmetry classification of modes in a one-dimensional (1D) \mathcal{PT} symmetric photonic lattice shown in Fig. 1(a). The approach is completely general and can be applied to \mathcal{PT} symmetric geometries with periodicity in any dimension. The general predictive power of the techniques presented here will help avoid numerous unnecessary computations and provide valuable insight in \mathcal{PT} symmetric photonic device design.

Heesh-Shubnikov groups [4, 5, 42] (also referred to as magnetic groups or color groups [43, 44]) will be used to provide a general description of the role of symmetry in determining whether eigenfunctions are expected to exhibit \mathcal{PT} -degeneracy with complex eigenfrequencies or are expected to be non-degenerate or classically degenerate with real eigenfrequencies. Heesh-Shubnikov groups describe the symmetry of regularly-shaped objects but whose components may have different colors. Examples include a square half of which is black and the other half is white or the *taijitu* (yin and yang) symbol [44]. The development of Heesh-Shubnikov groups was motivated by studies of magnetic ordering in ferromagnetic and ferroelectric materials [43–45]. In these lattices the periodically arranged identical atoms are not distinguished by color but, rather, by spin, and the same mathematical framework applies.

The electromagnetic wave equation in a source-free nonmagnetic medium in the frequency domain may be written as

$$\nabla \times \left[\frac{1}{\epsilon(\vec{r})} \nabla \times \vec{H}(\vec{r}) \right] = \Xi \vec{H}(\vec{r}) = \left(\frac{\omega}{c} \right)^2 \vec{H}(\vec{r}) \quad (1)$$

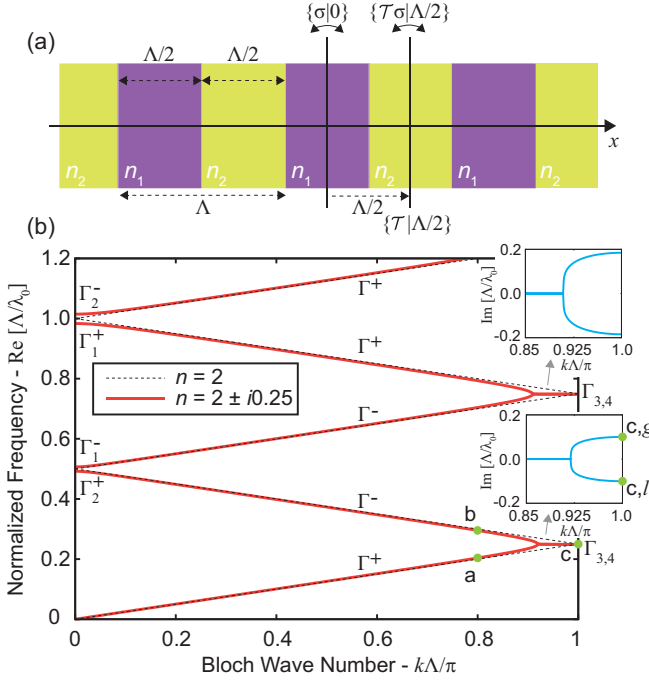


FIG. 1. (a) Schematic diagram showing the one-dimensional \mathcal{PT} symmetric photonic lattice. Regions labeled n_1 provide gain ($n_1 = n_r + in_i$), and regions labeled n_2 provide loss ($n_2 = n_r - in_i$) for positive n_r and n_i . Point and space group symmetry operations are labeled. (b) Photonic band diagram calculated using the plane wave expansion method. Dashed black line: empty lattice band diagram. Insets depict the imaginary part of the frequency for modes with \mathcal{PT} -degeneracy. λ_0 is the vacuum wavelength. Corepresentation labels correspond to the labels in Tables I and III and Table VIII in [46].

where c is the vacuum speed of light, and $\epsilon(\vec{r})$ is the relative permittivity. For \mathcal{PT} symmetric systems in which

$$[\mathcal{PT}, \Xi] = 0, \quad (2)$$

one has

$$\begin{aligned} \Xi \mathcal{PT} \vec{H}(\vec{r}) &= \mathcal{PT} \Xi \vec{H}(\vec{r}) = \mathcal{PT} \left(\frac{\omega}{c} \right)^2 \vec{H}(\vec{r}) \\ &= \left(\frac{\omega^*}{c} \right)^2 \mathcal{PT} \vec{H}(\vec{r}). \end{aligned} \quad (3)$$

So if $\vec{H}(\vec{r})$ is an eigenfunction with frequency ω , then $\mathcal{PT} \vec{H}(\vec{r})$ is also an eigenfunction but with frequency ω^* . The complex conjugation of the eigenvalue is typical of antilinear operators. \mathcal{PT} is also an antiunitary operation which excludes the application of representation theory based on classical groups. Rather, corepresentation theory based on Heesh-Shubnikov groups is required.

The symmetry elements of the 1D periodic \mathcal{PT} symmetric structure are shown in Fig. 1(a) and are given by

$e = \{E|0\}$, $m = \{\sigma|0\}$, $\xi = \{\mathcal{T}|a/2\}$, $\mu = \{\mathcal{T}\sigma|a/2\}$. Elements e and m are unitary operators, whereas ξ and μ are antiunitary due to the presence of \mathcal{T} . The breakdown of classical group theory when dealing with antiunitary operations is illustrated by considering the matrix representation of the operators. Let R_i denote the i th unitary operator (e or m) and let A_i denote the i th antiunitary operator (ξ or μ). Let $\Gamma(B)$ be the matrix representation of unitary or antiunitary operator B . Then the following classical conditions must hold for a valid group representation: $\Gamma(R_i)\Gamma(R_j) = \Gamma(R_i R_j)$ and $\Gamma(R_i)\Gamma(A_j) = \Gamma(R_i A_j)$. However, when an antiunitary representation occurs first on the left side, then the following conditions must hold $\Gamma(A_i)\Gamma(R_j)^* = \Gamma(A_i R_j)$ and $\Gamma(A_i)\Gamma(A_j)^* = \Gamma(A_i A_j)$. The complex conjugation of the second term spawns the development of the non-classical Heesh-Shubnikov group corepresentation theory [45].

Because $\xi\xi = \{E|a\}$ is a pure translation, the full space group must be employed. Based on the Bloch form for modes of periodic systems, one can use a representation of the space group, $\exp(ikna)$, where n is an integer [47, 48]. Application of space groups is facilitated by identification of the *little group* or group of \vec{k} which consists of symmetry operations which send \vec{k} into $\vec{k} + \vec{K}$ where \vec{K} is a reciprocal lattice vector [49, 50]. However, for *Heesh-Shubnikov little groups* that include antiunitary operators, such a group includes (i) unitary elements of the space group that send \vec{k} into $\vec{k} + \vec{K}$ (as before) and (ii) antiunitary elements of the space group that send \vec{k} into $-\vec{k} + \vec{K}$ [44].

For a 1D lattice $\vec{k} = \hat{x}k$, so for brevity we will proceed with the scalar part k . In the following we consider the Heesh-Shubnikov little group (HSLG) representations at high symmetry points $k = 0$ and $k = \pi/\Lambda$ and at a low symmetry point in the first Brillouin zone ($0 < k < \pi/\Lambda$). For $k = 0$, the space group representation takes on only one value ($\exp(i0na) = 1$), and the HSLG includes all of the symmetry operations $\mathcal{M}^{k=0} = (e, m, \xi, \mu)$. This group is isomorphic to $C_{2v}(2mm)$ and the *Viergruppe* [46, 50]. The elements $\mathcal{N} = (e, m)$ do not contain \mathcal{T} , and they form a unitary subgroup of index 2. This subgroup is isomorphic to $C_{1h}(m)$ [46, 50]. The antiunitary elements form a coset of \mathcal{N} : $A\mathcal{N}$ for $A \in (\xi, \mu)$. Therefore, this HSLG may be expressed as $\mathcal{M}^{k=0} = \mathcal{N} + A\mathcal{N} = C_{1h} + \{\mathcal{T}|\frac{\Lambda}{2}\}C_{1h}$. The final equality uses $A = \xi$ and helps illustrate the structure of the group. Ultimately the HSLG contains two C_{1h} symmetry centers offset by $\Lambda/2$ and distinguished by complex conjugation \mathcal{T} . Cracknell classifies Heesh-Shubnikov groups of this form as Type IV [43, 44].

Corepresentations of \mathcal{M} fall into three categories [45, 51]. To determine the category Dimmock and Wheeler [52] devised a sum rule similar to a rule obtained earlier by Frobenius and Schur [53]. The Dimmock and

Wheeler test is

$$\sum_{B \in \mathcal{W}} \chi(B^2) = \begin{cases} n & \text{Type (a),} \\ -n & \text{Type (b),} \\ 0 & \text{Type (c),} \end{cases} \quad (4)$$

where $\chi(R)$ is the character of the classical representation of R , n is the order of the unitary subgroup and \mathcal{W} is the set of antiunitary operators. Type (a) corepresentations correspond to a single representation of the unitary subgroup, and no new degeneracy is introduced. Type (b) corepresentations contain the same single representation of the unitary subgroup twice, and new degeneracy may appear. Type (c) corepresentations contain two inequivalent corepresentations of the unitary subgroup, and new degeneracy is introduced [45, 51]. The primary outcome of this work is that thresholdless \mathcal{PT} transitions are associated with Type (b) and (c) corepresentations, and modes with real frequency eigenvalues have Type (a) corepresentations.

TABLE I. Corepresentations of $\mathcal{M}^{k=0}$.

Correp.	$C_{1h}(m)$	e	m	ξ	μ
(a)	A', Γ_1^+	1	1	1	1
(a)	A', Γ_1^-	1	1	-1	-1
(a)	A'', Γ_2^+	1	-1	1	-1
(a)	A'', Γ_2^-	1	-1	-1	1

To continue with the symmetry analysis at $k = 0$, we perform the Dimmock and Wheeler test (Eq. 4). Squaring the antiunitary operators results in $(\xi^2, \mu^2) = (e, e)$ which yields two Type (a) corepresentations since $\chi(e) = 1$ [46, 50]. The components of the i th Type (a) corepresentation Γ_i for the unitary elements $R \in \mathcal{N}$ are given by $\Gamma_i(R) = \Delta_i(R)$ where $\Delta_i(R)$ is the i th classical representation of R in \mathcal{N} . The components of the i th Type (a) corepresentation Γ_i for the antiunitary elements $R \in \mathcal{W}$ are given by $\Gamma_i(RA) = \Delta_i(R)\beta$ where $A \in \mathcal{W}$ is an arbitrary but fixed antiunitary operator and $\beta\beta^* = \Delta_i(A^2)$ [45, 51]. Using $A = \xi$ results in $\beta\beta^* = \Delta_i(e) = 1$, so $\beta = \exp(\pm i\theta)$ (boldface removed to indicate scalar for the 1D corepresentation) with real θ , and the total number of corepresentations is doubled. Table I summarizes the results using $\beta = \pm 1$. A' and A'' label the classical representations of C_{1h} . Γ_i^\pm labels the corepresentations for $\beta = \pm 1$.

Because the corepresentations at $k = 0$ are all of Type (a), thresholdless \mathcal{PT} degeneracy is not expected to occur there. And because the classical representations of C_{1h} are all 1D, classical degeneracy is also not expected at $k = 0$. The band diagram obtained using the plane wave expansion method [49, 54] and shown in Fig. 1(b)

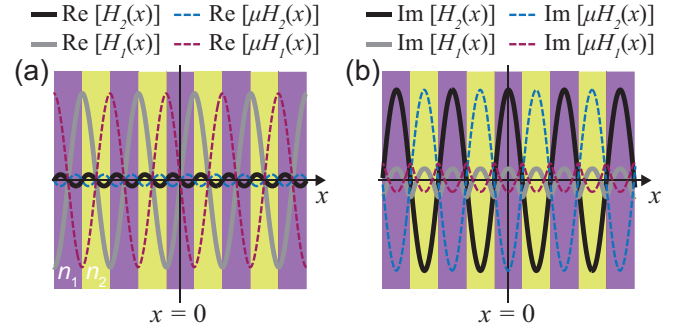


FIG. 2. Magnetic field ($H_z(x)$) spatial distribution in \mathcal{PT} symmetric 1D lattice at $k = 0$. H_1 corresponds to Γ_1^- labeled in Fig. 1(b), and H_2 corresponds to Γ_2^+ . Transformed fields are shown to verify the characters in Table I.

TABLE II. Character table of C_{2v} point group along with results of Dimmock and Wheeler test (α) and corepresentation type (Correp.).

$C_{2v}(2mm)$	e	\bar{e}	m	\bar{m}	α	Correp.
A_1	1	1	1	1	4	(a)
A_2	1	1	-1	-1	4	(a)
B_1	1	-1	1	-1	0	(c)
B_2	1	-1	-1	1	0	(c)

confirms this observation. Fig. 2 illustrates the fields for points labeled Γ_2^+ and Γ_1^- in Fig. 1(b) [46]. The character of the classical symmetry operations can be seen to be consistent with Table I. To illustrate the effect of an antiunitary operator, the result of operating with μ is shown; in both cases operating with μ reproduces the same function but multiplied by -1 which is consistent with Table I.

At $k = \pi/\Lambda$, the HSLG also includes all of the symmetry operations (e, m, ξ, μ) . But the space group representation $\exp(i\frac{\pi}{\Lambda}n\Lambda) = \exp(i\pi n) = 1$ for n even and -1 for n odd. To incorporate the properties of the space group, the symmetry elements are modified to $e = \{E|2n\Lambda\}$, $\bar{e} = \{E|2n\Lambda + \Lambda\}$, $m = \{\sigma|2n\Lambda\}$, $\bar{m} = \{\sigma|2n\Lambda + \Lambda\}$, $\xi = \{\mathcal{T}|2n\Lambda + \Lambda/2\}$, $\bar{\xi} = \{\mathcal{T}|2n\Lambda + \Lambda + \Lambda/2\}$, $\mu = \{\mathcal{T}\sigma|2n\Lambda + \Lambda/2\}$ and $\bar{\mu} = \{\mathcal{T}\sigma|2n\Lambda + \Lambda + \Lambda/2\}$. Therefore, the HSLG at $k = \pi/\Lambda$ is $\mathcal{M}^{k=\pi/\Lambda} = (e, \bar{e}, m, \bar{m}, \xi, \bar{\xi}, \mu, \bar{\mu})$ and is isomorphic to $C_{4v}(4mm)$ [46, 50]. The unitary subgroup of index 2 is $\mathcal{N} = (e, \bar{e}, m, \bar{m})$ and is isomorphic to $C_{2v}(2mm)$. This HSLG can be expressed as $\mathcal{M}^{k=\pi/\Lambda} = C_{2v} + \{\mathcal{T}|\frac{\Lambda}{2}\}C_{2v}$. The antiunitary elements are $\mathcal{W} = (\xi, \bar{\xi}, \mu, \bar{\mu})$. Squaring these elements results in $(\xi^2, \bar{\xi}^2, \mu^2, \bar{\mu}^2) = (\bar{e}, \bar{e}, e, e)$. Table II shows the character table for C_{2v} and the result of the Dimmock and Wheeler test $\alpha = \sum_{B \in \mathcal{W}} \chi(B^2)$. Representations A_1 and A_2 engender Type (a) corepresentations. Physically, we seek

TABLE III. Corepresentations of $\mathcal{M}^{k=\pi/\Lambda}$.

Correp.	$C_{2v}(2mm)$	e	\bar{e}	m	\bar{m}	ξ	$\bar{\xi}$	μ	$\bar{\mu}$
(a)	A_1, Γ_1	1	1	1	1	$(1)\beta$	$(1)\beta$	$(1)\beta$	$(1)\beta$
(a)	A_2, Γ_2	1	1	-1	-1	$(1)\beta$	$(1)\beta$	$(-1)\beta$	$(-1)\beta$
(c)	B_1, Γ_3	$\begin{pmatrix} 1 & 0 \\ 0 & 1 \end{pmatrix}$	$\begin{pmatrix} -1 & 0 \\ 0 & -1 \end{pmatrix}$	$\begin{pmatrix} 1 & 0 \\ 0 & -1 \end{pmatrix}$	$\begin{pmatrix} -1 & 0 \\ 0 & 1 \end{pmatrix}$	$\begin{pmatrix} 0 & 1 \\ -1 & 0 \end{pmatrix}$	$\begin{pmatrix} 0 & -1 \\ 1 & 0 \end{pmatrix}$	$\begin{pmatrix} 0 & 1 \\ 1 & 0 \end{pmatrix}$	$\begin{pmatrix} 0 & -1 \\ -1 & 0 \end{pmatrix}$
(c)	B_2, Γ_4	$\begin{pmatrix} 1 & 0 \\ 0 & 1 \end{pmatrix}$	$\begin{pmatrix} -1 & 0 \\ 0 & -1 \end{pmatrix}$	$\begin{pmatrix} -1 & 0 \\ 0 & 1 \end{pmatrix}$	$\begin{pmatrix} 1 & 0 \\ 0 & -1 \end{pmatrix}$	$\begin{pmatrix} 0 & 1 \\ -1 & 0 \end{pmatrix}$	$\begin{pmatrix} 0 & -1 \\ 1 & 0 \end{pmatrix}$	$\begin{pmatrix} 0 & -1 \\ -1 & 0 \end{pmatrix}$	$\begin{pmatrix} 0 & 1 \\ 1 & 0 \end{pmatrix}$

corepresentations that change sign upon application of e and \bar{e} . Therefore we discard on physical grounds the Type (a) corepresentations spawned by A_1 and A_2 . Further, assuming $A = \xi$, then $\beta\beta^* = \Delta_i(\bar{e}) = -1$. That there is no solution for β (boldface removed to indicate scalar for the 1D corepresentation) for these Type (a) 1D corepresentations is consistent with their unphysical nature. However, for completeness, we show all of the corepresentations in Table III.

Classical representations B_1 and B_2 engender Type (c) corepresentations. The components of the i th Type (c) corepresentation Γ_i for the unitary elements $R \in \mathcal{N}$ are given by [45, 51]

$$\Gamma_i(R) = \begin{pmatrix} \Delta(R) & \mathbf{0} \\ \mathbf{0} & \Delta^*(S^{-1}RS) \end{pmatrix} \quad (5)$$

where $A = S\mathcal{T}$. The components of the i th Type (c) corepresentation Γ_i for the antiunitary elements $R \in \mathcal{W}$ are given by

$$\Gamma_i(R) = \begin{pmatrix} \mathbf{0} & \Delta^*(A^{-1}R) \\ \Delta(RA) & \mathbf{0} \end{pmatrix}. \quad (6)$$

Details of the calculation are provided in [46], and the results make up the last two rows of Table III [51]. Corepresentations Γ_3 and Γ_4 are equivalent because they can be transformed into each other via $U\Gamma_3U^{-1} = \Gamma_4$ for the unitary elements and $U\Gamma_3(U^*)^{-1} = \Gamma_4$ for the antiunitary elements [45, 46, 51].

Because the $\Gamma_{3,4}$ corepresentation changes sign between e and \bar{e} , only this corepresentation is physically valid. Therefore, every $k = \pi/\Lambda$ eigenstate of the \mathcal{PT} symmetric 1D photonic lattice in Fig. 1(a) belongs to a two-dimensional (2D) Type (c) corepresentation. The photonic band structure displayed in Fig. 1(b) shows that coupled modes with complex conjugate eigenfrequencies form at every empty-lattice band crossing that occurs at $k = \pi/\Lambda$ [46]. Since every mode at $k = \pi/\Lambda$ exhibits a thresholdless \mathcal{PT} transition, we conclude that Type

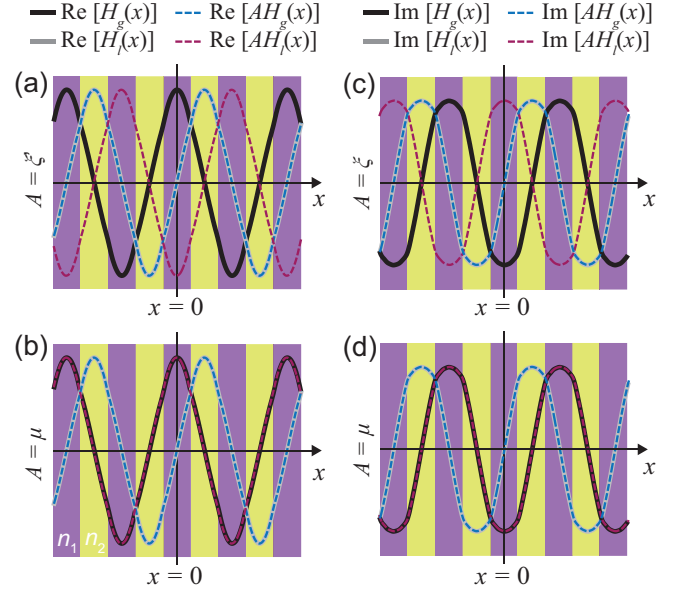


FIG. 3. Magnetic field ($H_z(x)$) spatial distribution in \mathcal{PT} symmetric 1D lattice at $k = \pi/\Lambda$ (point c in Fig. 1(b)). H_g corresponds to gain mode labeled c,g in Fig. 1(b), and H_l corresponds to the loss mode labeled c,l. Transformed fields are shown to verify the characters in Table III.

(c) 2D corepresentations are associated with thresholdless \mathcal{PT} -degeneracy.

In the \mathcal{PT} -degenerate regime, two coupled eigenstates have complex conjugate eigenfrequencies. Assuming a time-reference of $\exp(-i\omega t)$, the mode with positive imaginary frequency is the “gain mode”, and the mode with negative imaginary frequency is the “loss mode”. Figure 3 illustrates the spatial field distribution for the two modes at $k = \pi/\Lambda$ at the frequency $\Lambda/\lambda_0 \approx 0.25 \pm i0.1$ (indicated by the green dots labeled ‘c’, ‘c,g’ and ‘c,l’ in Fig. 1(b)). That these eigenfunctions possess the symmetry properties of the matrix corepresentations of the unitary operators shown in Table III is clear by inspection. To confirm that these modes also possess the symmetry properties of the matrix corepresentations of the antiunitary operators, ξ and μ were

applied to the gain and loss eigenfunctions. The transformed eigenfunction is represented by a dashed line. As predicted, the gain mode transforms into the loss mode for ξ and μ , and the loss mode transforms into the gain mode for μ and into its negative for ξ [46].

Finally, consider a wave vector at a low symmetry position in the first Brillouin zone (i.e. $k \neq 0, \pi/\Lambda$). For definiteness, we take $k = 0.8(\pi/\Lambda)$. In this case the only unitary operation that takes \vec{k} to $\vec{k} + \vec{K}$ is the identity E , and the only antiunitary operation that takes \vec{k} to $-\vec{k} + \vec{K}$ is μ . Because these symmetry operators do not result in pure translations, it is not necessary to employ the full space group. Performing the Dimmock and Wheeler test results in $\mu^2 = e$, so the corepresentations are all of Type (a), and no \mathcal{PT} -degeneracy is expected. The band diagram shown in Fig. 1(b) confirms this observation. The corepresentation table and depiction of the fields for $k = 0.8(\pi/\Lambda)$ (labeled ‘a’ and ‘b’ in Fig. 1(b)) are provided in [46].

Application of Heesh-Shubnikov groups to a \mathcal{PT} symmetric 1D lattice has allowed identification of points in the band diagram where thresholdless \mathcal{PT} -degeneracy is expected. Inspection of the band structure in Fig. 1(b) shows that there are \mathcal{PT} -degenerate modes for $k < \pi/\Lambda$. This is not expected based on symmetry. As pointed out previously [40], the \mathcal{PT} transition point shifts toward $k = 0$ as n_i is increased. At the \mathcal{PT} transition point, the modes with nominal Type (a) corepresentations transform into modes with Type (c) corepresentations. That this transition is a function of n_i , rather than symmetry, suggests that this phenomenon is indeed \mathcal{PT} symmetry breaking. As shown in [46] increasing the non-Hermiticity factor to $n_i = 0.7$ can transform the third and fourth bands at $k = 0$ from nominally Type (a) modes to Type (c) modes.

The use of Heesh-Shubnikov group theory has facilitated the classification of modes of 1D photonic lattices that possess \mathcal{PT} symmetry. We found points in the band structure in which thresholdless \mathcal{PT} -degeneracy occurs for every mode ($k = \pi/\Lambda$). Other than $k = \pi/\Lambda$, the modes are expected to be non-degenerate with real eigenvalues. However, symmetry can be broken in these structures, and \mathcal{PT} transitions are seen for $k < \pi/\Lambda$ and depend of the non-Hermiticity factor n_i . While a 1D lattice was the focus of this work, the approach is readily applicable to 2D and 3D photonic crystals where the variety of modes is even richer. Ultimately, we expect this analysis to be useful in the development of \mathcal{PT} symmetric photonic devices such as waveguides, cavities, delays and photonic crystal superprisms, to name a few.

in non-Hermitian Hamiltonians having \mathcal{PT} symmetry,” *Physical Review Letters* **80**, 5243–5246 (1998).

- [2] Carl M. Bender, Stefan Boettcher, and Peter N. Meisinger, “ \mathcal{PT} -symmetric quantum mechanics,” *Journal of Mathematical Physics* **40**, 2201–2229 (1999).
- [3] Carl M. Bender, Dorie C. Brody, and Hugh F. Jones, “Complex extension of quantum mechanics,” *Physical Review Letters* **89**, 270401 (2002).
- [4] H. Heesh, “Zur Strukturtheorie der ebenen Symmetriegruppen,” *Zeitschrift für Kristallographie-Crystalline Materials* **71**, 95–102 (1929).
- [5] A. V. Shubnikov and N. V. Belov, *Colored Symmetry* (Macmillan, 1964).
- [6] R. El-Ganainy, K. G. Makris, D. N. Christodoulides, and Ziad H. Musslimani, “Theory of coupled optical \mathcal{PT} -symmetric structures,” *Optics Letters* **32**, 2632–2634 (2007).
- [7] A. Guo, G. J. Salamo, D. Duchesne, R. Morandotti, M. Volatier-Ravat, V. Aimez, G. A. Siviloglou, and D. N. Christodoulides, “Observation of \mathcal{PT} -symmetry breaking in complex optical potentials,” *Physical Review Letters* **103**, 093902 (2009).
- [8] Ali Mostafazadeh, “Spectral singularities of complex scattering potentials and infinite reflection and transmission coefficients at real energies,” *Physical Review Letters* **102**, 220402 (2009).
- [9] Ali Mostafazadeh, “Resonance phenomenon related to spectral singularities, complex barrier potential, and resonating waveguides,” *Physical Review A* **80**, 032711 (2009).
- [10] Christian E. Rüter, Konstantinos G. Makris, Ramy El-Ganainy, Demetrios N. Christodoulides, Mordechai Segev, and Detlef Kip, “Observation of parity-time symmetry in optics,” *Nature Physics* **6**, 192–195 (2010).
- [11] Stefano Longhi, “ \mathcal{PT} -symmetric laser absorber,” *Physical Review A* **82**, 031801(R) (2010).
- [12] Jiří Čtyroký, Kuzmiak, Vladimír, and Sergey Eyderman, “Waveguide structures with antisymmetric gain/loss profile,” *Optics Express* **18**, 21585–21593 (2010).
- [13] Henri Benisty, Aloyse Degiron, Anatole Lupu, André De Lustrac, Sébastien Chénais, Sébastien Forget, Mondher Besbes, Grégory Barbillon, Surélien Bruyant, Blaize, Sylvain, and Gilles Lérondel, “Implementation of \mathcal{PT} symmetric devices using plasmonics: principle and applications,” *Optics Express* **19**, 18004–18019 (2011).
- [14] Li Ge, Y. D. Chong, and A. D. Stone, “Conservation relations and anisotropic transmission resonances in one-dimensional \mathcal{PT} -symmetric photonic heterostructures,” *Physical Review A* **85**, 023802 (2012).
- [15] Hossein Hodaei, Mohammad-Ali Miri, Matthias Heinrich, Demetrios N. Christodoulides, and Mercedeh Khajavikhan, “Parity-time-symmetric microring lasers,” *Science* **346**, 975–978 (2014).
- [16] Liang Feng, Zi Jing Wong, Ren-Min Ma, Yuan Wang, and Xiang Zhang, “Single-mode laser by parity-time symmetry breaking,” *Science* **346**, 972–975 (2014).
- [17] Stefano Longhi and Liang Feng, “ \mathcal{PT} -symmetric microring laser-absorber,” *Optics Letters* **39**, 5026–5029 (2014).
- [18] Long Chang, Xiaoshun Jiang, Shiyue Hua, Chao Yang, Jianming Wen, Liang Jiang, Guanyu Li, Guanzhong Wang, and Min Xiao, “Parity-time symmetry and variable optical isolation in active-passive-coupled microresonators,” *Nature Photonics* **8**, 524–529 (2014).

* mocklap@cmich.edu

[1] Carl M. Bender and Stefan Boettcher, “Real spectra

- [19] Bo Peng, Şahin Kaya Özdemir, Fuchuan Lei, Faraz Monifi, Mariagiovanna Gianfreda, Gui Lu Long, Shanhui Fan, Franco Nori, Carl M. Bender, and Lan Yang, “Parity-time-symmetric whispering-gallery micro cavities,” *Nature Physics* **10**, 394–398 (2014).
- [20] Sendy Phang, Ana Vukovic, Stephen C. Creagh, Trevor M. Benson, Phillip D. Sewell, and Gabriele Gradoni, “Parity-time symmetric coupled micro resonators with a dispersive gain/loss,” *Optics Express* **23**, 11493–11507 (2015).
- [21] Z. H. Musslimani, K. G. Makris, R. El-Ganainy, and D. N. Christodoulides, “Optical solitons in \mathcal{PT} periodic potentials,” *Physical Review Letters* **100**, 030402 (2008).
- [22] K. G. Makris, R. El-Ganainy, D. N. Christodoulides, and Z. H. Musslimani, “Beam dynamics in \mathcal{PT} symmetric optical lattices,” *Physical Review Letters* **100**, 103904 (2008).
- [23] Keya Zhou, Zhongyi Guo, Jicheng Wang, and Shutian Liu, “Defect modes in defective parity-time symmetric periodic complex potentials,” *Optics Letters* **35**, 2928–2930 (2010).
- [24] Zin Lin, Hamidreza Ramezani, Toni Eichelkraut, Tsampikos Kottos, Hui Cao, and Demetrios N. Christodoulides, “Unidirectional invisibility induced by \mathcal{PT} -symmetric periodic structures,” *Physical Review Letters* **106**, 213901 (2011).
- [25] Alexander Szameit, Mikael C. Rechtsman, Omri Bahat-Treidel, and Mordechai Segev, “ \mathcal{PT} -symmetry in honeycomb photonic lattices,” *Physical Review A* **84**, 021806 (2011).
- [26] Alois Regensburger, Christoph Bersch, Mohammad-Ali Miri, Georgy Onishchukov, Demetrios N. Christodoulides, and Ulf Peschel, “Parity-time synthetic photonic lattices,” *Nature* **488**, 167–171 (2012).
- [27] Liang Feng, Ye-Long Xu, William S. Fegadolli, Ming-Hui Lu, José E. B. Oliveira, Vilson R. Almeida, Yan-Feng Chen, and Axel Scherer, “Experimental demonstration of a unidirectional reflectionless parity-time metamaterial at optical frequencies,” *Nature Materials* **12**, 108–113 (2013).
- [28] Alois Regensburger, Mohammad-Ali Miri, Christoph Bersch, Jakob Näger, Georgy Onishchukov, Demetrios N. Christodoulides, and Ulf Peschel, “Observation of defect states in \mathcal{PT} -symmetric optical lattices,” *Physical review letters* **110**, 223902 (2013).
- [29] Hadiseh Alaieian and Jennifer A. Dionne, “Parity-time-symmetric plasmonic metamaterials,” *Physical Review A* **89**, 033829 (2014).
- [30] Xue-Feng Zhu, Yu-Gui Peng, and De-Gang Zhao, “Anisotropic reflection oscillation in periodic multilayer structures of parity-time symmetry,” *Optics Express* **22**, 18401–18411 (2014).
- [31] Jianing Xie, Zhikun Su, Weicheng Chen, Guojie Chen, Jiantao Lv, Dumitru Mihalache, and Yingji He, “Defect solitons in two-dimensional photonic lattices with parity-time symmetry,” *Optics Communications* **313**, 139–145 (2014).
- [32] Vassilios Yannopapas, “Spontaneous \mathcal{PT} -symmetry breaking in complex frequency band structures,” *Physical Review A* **89**, 013808 (2014).
- [33] Mykola Kulishov, Bernard Kress, and H. F. Jones, “Novel optical characteristics of a Fabry-Perot resonator with embedded \mathcal{PT} -symmetrical grating,” *Optics Express* **22**, 23164–23181 (2014).
- [34] Xue-Feng Zhu, “Defect states and exceptional point splitting in the band gaps of one-dimensional parity-time lattices,” *Optics Express* **23**, 22274–22284 (2015).
- [35] Li Ge, Konstantinos G. Makris, Demetrios N. Christodoulides, and Liang Feng, “Scattering in \mathcal{PT} - and \mathcal{RT} -symmetric multimode waveguides: Generalized conservation laws and spontaneous symmetry breaking beyond one dimension,” *Physical Review A* **92**, 062135 (2015).
- [36] Hong Wang, Shuang Shi, Xiaoping Ren, Xing Zhu, Boris A. Malomed, Dumitru Mihalache, and Yingji He, “Two-dimensional solitons in triangular photonic lattices with parity-time symmetry,” *Optics Communications* **335**, 146–152 (2015).
- [37] Kaustubh S. Agarwal, Rajeev K. Pathak, and Yogesh N. Joglekar, “Exactly solvable-symmetric models in two dimensions,” *Europhysics Letters* **112**, 31003 (2015).
- [38] Li Ge, “Parity-time symmetry in a flat-band system,” *Physical Review A* **92**, 052103 (2015).
- [39] Kun Ding, Z. Q. Zhang, and C. T. Chan, “Coalescence of exceptional points and phase diagrams for one-dimensional \mathcal{PT} -symmetric photonic crystals,” *Physical Review B* **92**, 235310 (2015).
- [40] Adam Mock, “Parity-time symmetry breaking in two-dimensional photonic crystals: square lattice,” *Physical Review A* **93**, 063812 (2016).
- [41] Alexander Cerjan, Aaswath Raman, and Shanhui Fan, “Exceptional contours and band structure design in parity-time symmetric photonic crystals,” *Physical Review Letters* **116**, 203902 (2016).
- [42] A. V. Shubnikov, *Symmetry and Antisymmetry of Finite Figures* (Izd-vo Akademii nauk SSSR, Moscow, 1951).
- [43] A. P. Cracknell, *Group Theory in Solid-State Physics* (Taylor and Francis, London, 1975).
- [44] A. P. Cracknell, *Magnetism in Crystalline Materials* (Pergamon Press, 1975).
- [45] Eugene P. Wigner, *Group Theory and its Application to the Quantum Mechanics of Atomic Spectra* (Academic Press, 1959).
- [46] See Supplemental Material for discussion of symmetry operators and eigenstates at $k = 0$, symmetry operators and eigenstates at $k = \pi/\Lambda$, construction of corepresentation table of $\mathcal{M}^{k=\pi/\Lambda}$, unitary matrix relating Γ_3 to Γ_4 , corepresentation table of $\mathcal{M}^{k=0.8(\pi/\Lambda)}$, and a discussion of broken \mathcal{PT} symmetry.
- [47] Volker Heine, *Group Theory in Quantum Mechanics* (Pergamon Press, New York, 1960).
- [48] Adam Mock, Ling Lu, and John O’Brien, “Space group theory and fourier space analysis of two-dimensional photonic crystal waveguides,” *Physical Review B* **81**, 155115 (2010).
- [49] Kazuaki Sakoda, *Optical Properties of Photonic Crystals* (Springer, Germany, 2001).
- [50] Michael Tinkham, *Group Theory and Quantum Mechanics* (Dover Publications, Inc., New York, 1964).
- [51] M. El-Batanouny and F. Wooten, *Symmetry and condensed matter physics: a computational approach* (Cambridge University Press, 2008).
- [52] J. O. Dimmock and R. G. Wheeler, “Symmetry properties of wave functions in magnetic crystals,” *Physical Review* **127**, 391–404 (1962).
- [53] G. Frobenius and I. Schur, “Über die reellen Darstellungen der endlichen Gruppen,” *Sitzungsberichte Der*

- Berliner Mathematischen Gesellschaft , 186–208 (1906).
- [54] M. Plihal, A. Shambrook, A. A. Maradudin, and Ping Sheng, “Two-dimensional photonic band structures,” *Optics Communications* **80**, 199–204 (1991).

Supplemental Material For
Characterization of Parity-Time Symmetry in Photonic Lattices Using
Heesh-Shubnikov Group Theory

Adam Mock

School of Engineering and Technology, Central Michigan University, ET 100, Mount Pleasant, MI
48859, USA

and Science of Advanced Materials Program Central Michigan University, Mount Pleasant, MI
48859, USA

1. Symmetry operators at $k = 0$

The group multiplication for the Heesh-Shubnikov little group (HSLG) of $k = 0$, $\mathcal{M}^{k=0} = (e, m, \xi, \mu)$, is provided below. Because $k = 0$, the space group representation does not play a role. $\mathcal{M}^{k=0}$ is isomorphic to $C_{2v}(2mm)$.

TABLE I. Multiplication table for $\mathcal{M}^{k=0}$.

$C_{2v}(2mm)$	e	m	ξ	μ
e	e	m	ξ	μ
m	m	e	μ	ξ
ξ	ξ	μ	e	m
μ	μ	ξ	m	e

The unitary subgroup of $\mathcal{M}^{k=0}$ is isomorphic to $C_{1h}(m)$.

TABLE II. Multiplication table for unitary subgroup of $\mathcal{M}^{k=0}$.

$C_{1h}(m)$	e	m
e	e	m
m	m	e

2. Discussion of modes at $k = 0$

To provide some insight into the lack of \mathcal{PT} degeneracy at $k = 0$, consider the effect of ξ on an eigenfunction at $k = 0$: $\xi H^{0,i}(x) = [H^{0,i}(x - \Lambda/2)]^*$ where $H^{0,i}(x)$ is the eigenfunction of the i th band at $k = 0$. From Table I in the main text we know that $\xi H^{0,i}(x) = \pm H^{0,i}(x)$, so we conclude $\pm H^{0,i}(x) = [H^{0,i}(x - \Lambda/2)]^*$. The implication is that the field intensity $|H^{0,i}(x)| =$

TABLE III. Character table of $C_{1h}(m)$ point group along with results of Dimmock and Wheeler test (α) and corepresentation type (Correp.).

$C_{1h}(m)$	e	m	α	Correp.
A'	1	1	2	(a)
A''	1	-1	2	(a)

$|[H^{0,i}(x - \Lambda/2)]^*| = |H^{0,i}(x - \Lambda/2)|$ is spatially periodic with a period of $\Lambda/2$. With this periodicity, spatially shifting an eigenfunction by $\Lambda/2$ reproduces the same field intensity instead of transforming into a field intensity with a different preferential overlap with the gain or loss regions. Therefore, these modes overlap the gain and loss regions equally which results in real eigenfrequencies. The $\Lambda/2$ periodicity of $|H^{0,i}(x)|$ is apparent in the fields shown in Fig. 2 in the main text.

3. Symmetry operators at $k = \pi/\Lambda$

At $k = \pi/\Lambda$, the space group representation plays a role in the analysis. Space group operations are described by the Seitz operator $\{R|t\}$ which consists of a point symmetry operation R followed by a translation t . The multiplication operation between Seitz operators is given by

$$\{R|t\}\{S|t'\} = \{RS|Rt' + t\}$$

As example consider $\bar{e}m = \{E|2m\Lambda + \Lambda\}\{\sigma|2n\Lambda\} = \{\sigma|2(m+n)\Lambda + \Lambda\} \equiv \{\sigma|2n\Lambda + \Lambda\} = \bar{m}$ where we have noted that a translation of $2(m+n)\Lambda$ is equivalent to $2n\Lambda$ for integer m and n at $k = \frac{\pi}{\Lambda}$. Consider now $m\bar{e} = \{\sigma|2n\Lambda\}\{E|2m\Lambda + \Lambda\} = \{\sigma|\sigma(2m\Lambda + \Lambda) + 2n\Lambda\} = \{\sigma|-(2m\Lambda + \Lambda) + 2n\Lambda\} = \{\sigma|2(n-m)\Lambda - \Lambda\} \equiv \{\sigma|2n\Lambda + \Lambda\} = \bar{m}$.

When the Seitz operator contains the time inversion operation \mathcal{T} , it applies only to other time inversion operators and not to the point and spatial symmetry operations. As example consider $m\mu = \{\sigma|2m\Lambda\}\{\mathcal{T}\sigma|2n\Lambda + \Lambda/2\} = \mathcal{T}\{\sigma\sigma|2m\Lambda + \sigma(2n\Lambda + \Lambda/2)\} = \mathcal{T}\{E|2m\Lambda - (2n\Lambda + \Lambda/2)\} = \{\mathcal{T}|2(m-n)\Lambda - \Lambda/2\} = \{\mathcal{T}|2(m-n-1)\Lambda + \Lambda + \Lambda/2\} \equiv \{\mathcal{T}|2n\Lambda + \Lambda + \Lambda/2\} = \bar{\xi}$.

Table IV shows the group multiplication table of the HSLG of $k = \frac{\pi}{\Lambda}$, $\mathcal{M}^{k=\pi/\Lambda}$. $\mathcal{M}^{k=\pi/\Lambda}$ is isomorphic to $C_{4v}(4mm)$.

TABLE IV. Multiplication table for $\mathcal{M}^{k=\pi/\Lambda}$.

$C_{4v}(4mm)$	e	\bar{e}	m	\bar{m}	ξ	$\bar{\xi}$	μ	$\bar{\mu}$
e	e	\bar{e}	m	\bar{m}	ξ	$\bar{\xi}$	μ	$\bar{\mu}$
\bar{e}	\bar{e}	e	\bar{m}	m	$\bar{\xi}$	ξ	$\bar{\mu}$	μ
m	m	\bar{m}	e	\bar{e}	$\bar{\mu}$	μ	$\bar{\xi}$	ξ
\bar{m}	\bar{m}	m	\bar{e}	e	μ	$\bar{\mu}$	ξ	$\bar{\xi}$
ξ	ξ	$\bar{\xi}$	μ	$\bar{\mu}$	\bar{e}	e	\bar{m}	m
$\bar{\xi}$	$\bar{\xi}$	ξ	$\bar{\mu}$	μ	e	\bar{e}	m	\bar{m}
μ	μ	$\bar{\mu}$	ξ	$\bar{\xi}$	m	\bar{m}	e	\bar{e}
$\bar{\mu}$	$\bar{\mu}$	μ	$\bar{\xi}$	ξ	\bar{m}	m	\bar{e}	e

 TABLE V. Multiplication table for unitary subgroup of $\mathcal{M}^{k=\pi/\Lambda}$. It is isomorphic to $C_{2v}(2mm)$.

$C_{2v}(2mm)$	e	\bar{e}	m	\bar{m}
e	e	\bar{e}	m	\bar{m}
\bar{e}	\bar{e}	e	\bar{m}	m
m	m	\bar{m}	e	\bar{e}
\bar{m}	\bar{m}	m	\bar{e}	e

4. Construction of corepresentation table for $\mathcal{M}^{k=\pi/\Lambda}$

Here we provide calculation details for the construction of the corepresentation table for the group $\mathcal{M}^{k=\pi/\Lambda}$. For Type (a) corepresentations, the elements of the unitary subgroup retain their classical representations $\Gamma_i(R) = \Delta_i(R)$ for $R \in \mathcal{N}$.

Corepresentations of the antiunitary elements are given in terms of the classical representations of the unitary subgroup according to $\Gamma_i(RA) = \Delta_i(R)\beta$ with $\beta\beta^* = \Delta_i(A^2)$. Here we choose $A = \xi$. Using a different operator for A will give the same results.

$$\Gamma_i(\xi e) = \Gamma_i(\xi) = \Delta_i(e)\beta$$

$$\Gamma_i(\xi \bar{e}) = \Gamma_i(\bar{\xi}) = \Delta_i(\bar{e})\beta$$

$$\Gamma_i(\xi m) = \Gamma_i(\mu) = \Delta_i(m)\beta$$

$$\Gamma_i(\xi \bar{m}) = \Gamma_i(\bar{\mu}) = \Delta_i(\bar{m})\beta$$

The classical representations of the group C_{2v} are provided in Table II in the main text. The corepresentations resulting from this calculation make up the first two rows of Table III in the main text.

For Type (c) corepresentations, the corepresentations of the elements of the unitary subgroup are given by Eq. 5 in the main text. With $A = \xi = S\mathcal{T}$, we identify $S = \{E|2n\Lambda + \Lambda/2\}$ and $S^{-1} = \{E|-2n\Lambda - \Lambda/2\}$. Determination of the matrix elements is shown in Table VI.

TABLE VI. Determination of the matrix elements for the Type (c) corepresentations of the unitary operators in $\mathcal{M}^{k=\pi/\Lambda}$

R	RS	$S^{-1}RS$
e	$\{E 2n\Lambda + \Lambda/2\}$	$\{E 0\} = e$
\bar{e}	$\{E 2n\Lambda - \Lambda/2\}$	$\{E -\Lambda\} = \bar{e}$
m	$\{\sigma -\Lambda/2\}$	$\{\sigma -2n\Lambda - \Lambda\} = \bar{m}$
\bar{m}	$\{\sigma \Lambda/2\}$	$\{\sigma -2n\Lambda\} = m$

For Type (c) corepresentations, the corepresentations of the antiunitary elements are given by Eq. 6 in the main text. With $A = \xi$, we identify $A^{-1} = \bar{\xi}$. Determination of the matrix elements is shown in Table VII.

TABLE VII. Determination of the matrix elements for the Type (c) corepresentations of the antiunitary operators in $\mathcal{M}^{k=\pi/\Lambda}$.

B	BA	$A^{-1}B$
ξ	\bar{e}	e
$\bar{\xi}$	e	\bar{e}
μ	m	m
$\bar{\mu}$	\bar{m}	\bar{m}

The corepresentations resulting from this calculation make up the last two rows of Table III in the main text.

5. Unitary matrix that transforms Γ_3 into Γ_4 at $k = \pi/\Lambda$.

Corepresentations Γ_3 and Γ_4 are equivalent because they can be transformed into each other via $U\Gamma_3U^{-1} = \Gamma_4$ for the unitary elements and $U\Gamma_3(U^*)^{-1} = \Gamma_4$ for the antiunitary elements. Any

matrix of the form

$$U = \begin{pmatrix} 0 & -e^{-i\theta} \\ e^{i\theta} & 0 \end{pmatrix}$$

accomplishes this transformation for real θ .

6. Discussion of modes at $k = \pi/\Lambda$.

Using the gain and loss modes ($H_g^{k,i}(x)$ and $H_l^{k,i}(x)$, respectively) as a basis of the corepresentation at wave number $k = \pi/\Lambda$ and empty-lattice band crossing point i , Table III in the main text shows that when the unitary symmetry operators (R) are applied, the eigenfunctions transform according to diagonal matrices

$$R \begin{pmatrix} H_g^{k,i}(x) \\ H_l^{k,i}(x) \end{pmatrix} = \begin{pmatrix} r_{11} & 0 \\ 0 & r_{22} \end{pmatrix} \begin{pmatrix} H_g^{k,i}(x) \\ H_l^{k,i}(x) \end{pmatrix} = \begin{pmatrix} r_{11} H_g^{k,i}(x) \\ r_{22} H_l^{k,i}(x) \end{pmatrix}$$

showing that application of R to the 2D basis does not mix or exchange the eigenfunctions. This is to be contrasted to the transformation of the eigenfunctions upon application of the antiunitary operators (A) which are represented by anti-symmetric matrices:

$$A \begin{pmatrix} H_g^{k,i}(x) \\ H_l^{k,i}(x) \end{pmatrix} = \begin{pmatrix} 0 & a_{12} \\ a_{21} & 0 \end{pmatrix} \begin{pmatrix} H_g^{k,i}(x) \\ H_l^{k,i}(x) \end{pmatrix} = \begin{pmatrix} a_{12} H_l^{k,i}(x) \\ a_{21} H_g^{k,i}(x) \end{pmatrix}.$$

Here it is seen that application of the antiunitary operator transforms a loss mode *into* a gain mode and vice versa. As discussed previously [40] gain and loss modes have similar symmetry, and if only the field intensity is visualized, the difference between them is a spatial shift such that the gain modes preferentially overlap the gain regions, and the loss modes preferentially overlap the loss regions. Because the antiunitary operators include this spatial shift, the mode transformation properties of the matrix corepresentations make physical sense.

7. Corepresentation for $\mathcal{M}^{k=0.8(\pi/\Lambda)}$

Corepresentation for $\mathcal{M}^{k=0.8(\pi/\Lambda)}$ are Type (a). Using $A = \mu$ yields $\beta\beta^* = \Delta_i(\mu^2) = 1$, so use $\beta = \pm 1$.

$$\Gamma_i(R\mu) = \Gamma_i(e\mu) = \Delta_i(e)\beta = \beta = \pm 1.$$

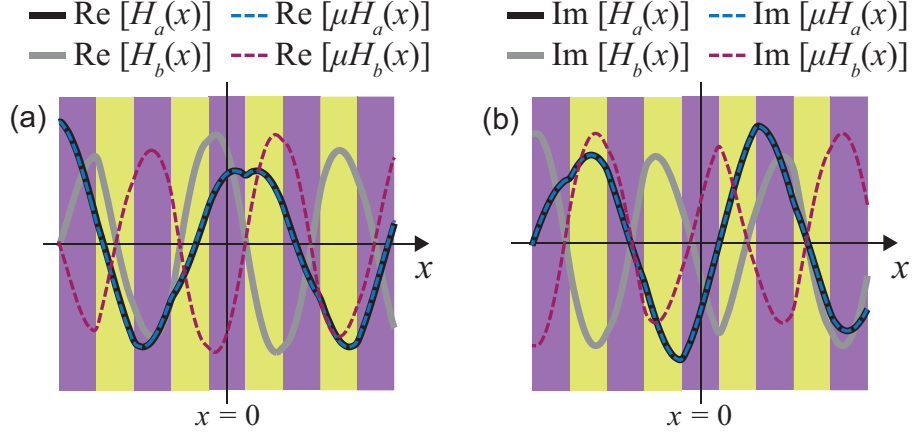


FIG. 1. Magnetic field ($H_z(x)$) spatial distribution in \mathcal{PT} symmetric 1D lattice at $k = 0.8(\pi/\Lambda)$ (points a and b in Fig. 2(b) in the main text). Transformed fields are shown to verify the characters in Table VIII.

Inspection of the fields in Fig. 1 indicates that H_a has corepresentation Γ^+ , and H_b has corepresentation Γ^- .

TABLE VIII. Corepresentations of $\mathcal{M}^{k=0.8(\pi/\Lambda)}$.

Correp.	$C_1(1)$	e	μ
(a)	A, Γ^+	1	1
(a)	A, Γ^-	1	-1

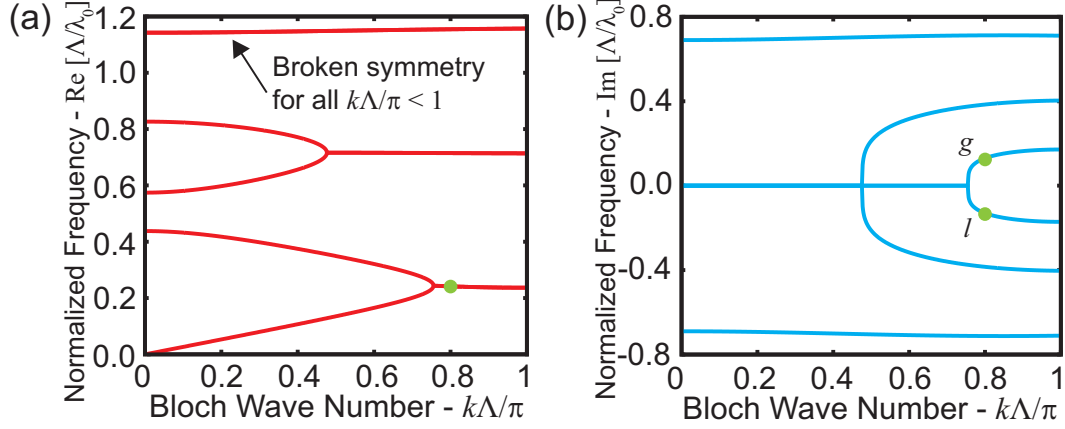


FIG. 2. Photonic band diagram for the 1D photonic lattice shown in Fig. 1(a) in the main text with $n = 2 \pm i0.7$. (a) Real part of the frequencies. (b) Imaginary part of the frequencies.

8. Broken \mathcal{PT} symmetry

Fig. 2 shows a band diagram for the 1D photonic lattice shown in Fig. 1(a) in the main text but with $n = 2 \pm i0.7$. This larger value for n_i results in \mathcal{PT} transition points closer to $k = 0$ than in Fig. 1(b). In fact for the fifth and sixth bands, the \mathcal{PT} transition point has reached $k = 0$, and these bands exhibit broken \mathcal{PT} symmetry for $0 \leq k < \pi/\Lambda$.

Fig. 3 shows the spatial field distribution for the modes marked by a circle at $k = 0.8(\pi/\Lambda)$ in Fig. 2(a) and labeled g and l in Fig. 2(b). When $n_i = 0.25$, the fields at $k = 0.8(\pi/\Lambda)$ are shown in Fig. 1, and the characters in Table VIII accurately describe the symmetry of the fields. When $n_i = 0.70$, the field symmetry is no longer of Type (a), and the mode is in the broken \mathcal{PT} symmetry regime. As shown in Fig. 3, the fields have Type (c) corepresentations where the antiunitary operator has a matrix corepresentation of the form

$$\mu = \begin{pmatrix} 0 & 1 \\ 1 & 0 \end{pmatrix}$$

This matrix is determined from observation of the field and does not follow from symmetry analysis.

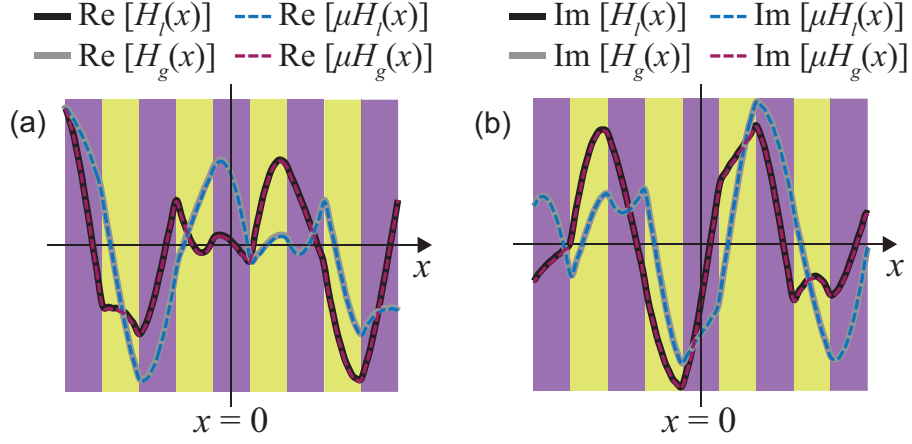


FIG. 3. Magnetic field ($H_z(x)$) spatial distribution in \mathcal{PT} symmetric 1D lattice with $n_i = 0.70$ at $k = 0.8(\pi/\Lambda)$ (point marked by a circle in Fig. 2). Transformed fields are shown to illustrate that mode symmetry differs from that predicted by group theory.